Published OnlineFirst March 16, 2015; DOI: 10.1158/1078-0432.CCR-14-2685

Cancer Therapy: Preclinical

Clinical Cancer Research

The MET Inhibitor AZD6094 (Savolitinib, HMPL-504) Induces Regression in Papillary Renal Cell Carcinoma Patient–Derived Xenograft Models

Alwin G. Schuller[1], Evan R. Barry[1], Rhys D.O. Jones[2], Ryan E. Henry[1], Melanie M. Frigault[1], Garry Beran[3], David Linsenmayer[1], Maureen Hattersley[1], Aaron Smith[2], Joanne Wilson[2], Stefano Cairo[4], Olivier Déas[4], Delphine Nicolle[4], Ammar Adam[1], Michael Zinda[1], Corinne Reimer[1], Stephen E. Fawell[1], Edwin A. Clark[1], and Celina M. D'Cruz[1]

Abstract

Purpose: Papillary renal cell carcinoma (PRCC) is the second most common cancer of the kidney and carries a poor prognosis for patients with nonlocalized disease. The HGF receptor MET plays a central role in PRCC and aberrations, either through mutation, copy number gain, or trisomy of chromosome 7 occurring in the majority of cases. The development of effective therapies in PRCC has been hampered in part by a lack of available preclinical models. We determined the pharmacodynamic and antitumor response of the selective MET inhibitor AZD6094 in two PRCC patient-derived xenograft (PDX) models.

Experimental Design: Two PRCC PDX models were identified and MET mutation status and copy number determined. Pharmacodynamic and antitumor activity of AZD6094 was tested using a dose response up to 25 mg/kg daily, representing clinically achievable exposures, and compared with the activity of the RCC standard-of-care sunitinib (in RCC43b) or the multikinase inhibitor crizotinib (in RCC47).

Results: AZD6094 treatment resulted in tumor regressions, whereas sunitinib or crizotinib resulted in unsustained growth inhibition. Pharmacodynamic analysis of tumors revealed that AZD6094 could robustly suppress pMET and the duration of target inhibition was dose related. AZD6094 inhibited multiple signaling nodes, including MAPK, PI3K, and EGFR. Finally, at doses that induced tumor regression, AZD6094 resulted in a dose- and time-dependent induction of cleaved PARP, a marker of cell death.

Conclusions: Data presented provide the first report testing therapeutics in preclinical *in vivo* models of PRCC and support the clinical development of AZD6094 in this indication. *Clin Cancer Res; 21(12); 2811–9. ©2015 AACR.*

Introduction

The hepatocyte growth factor (HGF) receptor MET is a membrane-associated receptor tyrosine kinase implicated in many human malignancies, including papillary renal cell carcinoma (PRCC; refs. 1–3). MET is a heterodimer consisting of a short extracellular α chain disulfide-linked to a larger β chain which includes extracellular, transmembrane, and intracellular regions. Binding of HGF, the MET ligand, leads to receptor oligomerization and autophosphorylation at tyrosine 1234 and 1235 within the kinase domain, resulting in the activation of several downstream pathways, including the RAS–RAF–MAPK pathway, PI3K signaling, Shp2, PLCγ, STAT3, and Crk. Therefore, activation of MET promotes diverse and context-dependent physiologic responses. Uncontrolled MET signaling can be achieved through several molecular mechanisms, including overexpression of MET or its ligand HGF, activating mutations, and amplification of the *MET* gene. As such, the MET signaling pathway has been recognized as an attractive target in RCC (4). In addition, heterodimerization with other RTKs, including EGFR, HER2, HER3, and RET, has been proposed as a means to activate MET signaling in cancer (5).

PRCC is the second most common cancer of the renal tubes comprising approximately 10% to 15% of renal cancers in the United States (6). PRCC presents as either a sporadic or inherited disease marked by high incidence (~75%) of chromosome 7 trisomy or tetrasomy, where genes for the MET receptor tyrosine kinase and HGF reside (7). Activating mutations in the kinase domain of MET are found in the majority of hereditary PRCC cases, as well as approximately 5% to 13% of sporadic PRCC cases (8). In addition, a large molecular study recently analyzed 220 samples from sporadic PRCC patients describing high MET expression levels across all PRCC samples. Of note, although no samples were identified as amplified (defined as over 5 copies), MET copy number gain was observed in both of the distinct pathologic subtypes of PRCC (81% of type I and 46% of type II PRCC; ref. 9). Together, these data suggest an oncogenic role for MET in PRCC.

Currently available therapies for PRCC unfortunately provide only modest benefit. Sunitinib, which is approved by the FDA for RCC, achieves response rates of only approximately 11% in

[1]Oncology Innovative Medicines, AstraZeneca, Waltham, Massachusetts. [2]AstraZeneca, Cambridge, United Kingdom. [3]AstraZeneca, Alderley Park, United Kingdom. [4]Xentech, Evry, France.

Note: Supplementary data for this article are available at Clinical Cancer Research Online (http://clincancerres.aacrjournals.org/).

Corresponding Author: Celina D'Cruz, AstraZeneca, Gatehouse Park, Waltham, MA SK10 4TG. Phone: 781-839-4234; Fax: 781-839-4210; E-mail: Celina.Dcruz@astrazeneca.com

doi: 10.1158/1078-0432.CCR-14-2685

©2015 American Association for Cancer Research.

Downloaded from clincancerres.aacrjournals.org on January 12, 2016. © 2015 American Association for Cancer Research.

Published OnlineFirst March 16, 2015; DOI: 10.1158/1078-0432.CCR-14-2685

Translational Relevance

Papillary renal cell cancer (PRCC) is a subset of renal cell cancer (RCC) with poor prognosis for patients with non-localized disease. Current treatment options, including the standard of care for RCC, provide only modest benefit. Recently, the molecular underpinnings of clinical PRCC have been evaluated describing a central role for MET. We utilized two independent patient derived PRCC xenograft models, both harboring MET copy number gain similar to that seen in patients, for therapeutic testing. We demonstrate that targeted agents for MET inhibition, including AZD6094 (Savolitinib, HMPL-504) induce tumor regressions and may be more efficacious than current therapeutic approaches warranting further clinical investigation.

non–clear cell RCC and median progression-free survival of 7.8 months (10) underscoring the need for novel therapeutic options in PRCC.

AZD6094 (savolitinib, HMPL-504) is a novel, potent, and selective MET inhibitor currently in clinical development in various indications, including PRCC (11, 12). In preclinical studies, AZD6094 displayed nanomolar *in vitro* activity against MET and its downstream signaling targets. *In vivo*, AZD6094 induced antitumor activity, particularly in tumor models with high MET gene amplification, including gastric cancer (SNU-5 and Hs746T) xenografts (12).

Overall, there is a lack of preclinical models of human PRCC for basic research and pharmaceutical development and therefore little comparative data of novel targeted therapies exist. Here, we present *in vivo* pharmacokinetic, pharmacodynamic, and antitumor activity data of AZD6094 in two patient-derived xenograft (PDX) models. We also compare the antitumor activity of AZD6094 to that of the multitargeted receptor tyrosine kinase inhibitor sunitinib (FDA-approved for renal cell cancer) and the ALK/ROS/MET kinase inhibitor crizotinib (FDA-approved for ALK-positive NSCLC). We observed that AZD6094 was more potent at clinically relevant doses than both crizotinib and sunitinib, warranting further development of AZD6094 in this indication.

Materials and Methods

Animals

Female athymic nude mice (Hsd:Athymic Nude-Fox1nu) were obtained from Harlan Laboratories and housed in pathogen-free animal housing at the Center for Exploration and Experimental Functional Research (CERFE, Evry, France) animal facility in individually ventilated cages (IVC) of polysulfone (PSU) plastic (mm 213 W × 362 D × 185 H) with sterilized and dust-free bedding cobs, access to sterilized food and water *ad libitum*, under a light–dark cycle (14-hour circadian cycle of artificial light) and controlled room temperature and humidity. Mice were housed in groups of maximum of 7 animals during 7 day acclimation period, and of a maximum of 6 animals during the experimental phase. All experiments were performed in accordance with French legislation concerning the protection of laboratory animals and in accordance with a currently valid license for experiments on vertebrate animals, issued by the French Ministry for Agriculture and Fisheries to Delphine Nicolle (No. C 91-570 dated May 31, 2011; validity: 5 years) as well as AstraZeneca Institutional Animal Care and Use Committee guidelines.

RCC-43b and RCC-47 PRCC PDX models

PDXs from donor mice reaching approximately 1,000 to 2,000 mm^3 were aseptically excised and dissected into fragments of approximately 20 mm^3 and transferred to culture medium before subcutaneous implantation into receiving mice (anesthetized with ketamine/xylazine, skin aseptized with a chlorhexidine solution, incised at the level of the interscapular region). All tumor fragments were obtained from the same passage and all mice were implanted on the same day.

Once tumors reached a size of approximately 60 to 200 mm^3 (14 days after implant for RCC-43b and 5 days after implant for RCC-47), mice were randomized into groups of 10 and dosed with vehicle, AZD6094 (2.5, 10, and 25 mg/kg, *per os*, daily, in acidic CMC-Na 0.5%, pH = 2.1), sunitinib (10 and 80 mg/kg, *per os*, daily, in 0.5% CMC (Sigma C9481), 0.9% NaCl, 0.4% polysorbate 80, 0.9% benzyl alcohol in water), or crizotinib (2.5 and 25 mg/kg, *per os*, daily, in water pH adjusted to 2.0).

Tumor diameters were measured by calliper three times a week during the treatment period and tumour volume (TV) calculated using the formula TV (mm^3) = [length (mm) × width (mm)2]/2 was used, where the length and the width were considered as the longest and the shortest diameters of the tumor, respectively. All animals were monitored daily and weighed three times a week during the treatment period.

Molecular analysis of PDX models

Genome-wide human SNP Array 6.0 from Affymetrix was used to determine the ploidy of the genome of the models RCC-43b (passage 4) and RCC-47 (passage 7) at Xentech Inc. Models have been previously characterized elsewhere (13) and RCC-43b (current Xentech nomenclature) has been referred to as RCC43 and RCC43-II in earlier publications. A GISTIC analysis of the $\log_2$ ratio with a cutoff of 0.7 was used to highlight chromosomal regions with at least 1 gene copy number gain or loss.

FISH analysis using a MET gene probe and CEP7 probe (RUO, Abbott) was used to determine the MET gene copy number from formalin-fixed paraffin-embedded sections of both models RCC-43b and RCC-47.

Pharmacodynamic/pharmacokinetic analysis

For single dose and end of study pharmacokinetic analysis, whole blood was collected under xylazine–ketamine anaesthesia by cardiac puncture, transferred to Microtainer lithium heparinate tubes, centrifuged at 5,000 rpm at room temperature for 5 minutes, and resulting plasma collected in polypropylene tubes and frozen at −80°C until shipment on dry ice and analysis.

Plasma samples were analyzed for parent only using a protein precipitation extraction procedure, followed by LC/MS-MS detection following the procedure below.

A stock (2 mmol/L) of the analytical standard (AZD6094) was prepared using DMSO and used on the Hamilton Star liquid handling platform to produce spiking solutions. A total of 23.75 μL of the required blank matrix was aliquoted into a 96-well plate. The matrix was spiked with 1.25 μL of each dilution to give a final concentration range of 1 nmol/L to 10,000 nmol/L. A total of 25 μL of each sample and standard were quenched with 100 μL of acetonitrile with internal standard, mixed, and centrifuged at 3,000 rpm for 15 minutes. Fifty microliters of the supernatant

Downloaded from clincancerres.aacrjournals.org on January 12, 2016. © 2015 American Association for Cancer Research.

Published OnlineFirst March 16, 2015; DOI: 10.1158/1078-0432.CCR-14-2685

was diluted 10-fold with deionized water and the samples were analyzed by LC/MS-MS using Masslynx and processed using Targetlynx. Pharmacokinetic parameters were generated using Phoenix 6.3.0.395.

Tumors were dissected, snap-frozen in liquid nitrogen, and frozen at −80°C until shipment on dry ice and analysis. Total MET and p-Y1349 was measured by MSD per manufacturer instructions. Tumor fragments were homogenized in lysis buffer containing Complete Protease Inhibitor Cocktail Tablets (Roche), Phosphatase Inhibitor Cocktail 2 (Sigma-Aldrich), Phosphatase Inhibitor Cocktail 3 (Sigma-Aldrich) using a Fisher Scientific Tissuemiser Homogenizer. Plates were blocked for 1 hour at room temperature, washed three times in Tris washing buffer, incubated with 25 μL of tumor samples for 1 hour at room temperature, washed three times in Tris washing buffer, incubated with 25 μL of detection antibody for 1 hour at room temperature, washed three times in Tris washing buffer before adding read buffer and reading signal on a SECTOR Imager 6000 (Meso Scale Discovery). Signals of triplicate samples were expressed relative to vehicle control samples. Potential changes in signaling molecules were analyzed by Western blot analysis. Tumor fragments were homogenized in lysis buffer containing Complete Protease Inhibitor Cocktail Tablets (Roche), Phosphatase Inhibitor Cocktail 2 (Sigma-Aldrich), Phosphatase Inhibitor Cocktail 3 (Sigma-Aldrich), using a Fisher Scientific Tissuemiser Homogenizer, proteins separated by SDS-PAGE, transferred to nitrocellulose membranes, and incubated with the following antibodies (all at 1:1,000 in TBST BSA 3%): pMET (Y1234/1235) Cell Signaling Technology (CST) 3077, MET CST 8198, EGFR CST 2232L, pEGFR (Y1068) CST 3777, pan-AKT CST 4685, pAKT (S473) CST 4060, ERK1/2 CST 9107, pERK1/2 (Thr202/Thr204) CST, STAT3 CST 4904S, pSTAT3 (Y705) CST 9145, PARP1 9532, followed by incubation with a secondary HRP-conjugated antibody and chemiluminescence detection.

Results

Identification of PDX models representing a subset of PRCC patient population

To identify representative preclinical models of the PRCC patient population, we analyzed genomic data from previously described PRCC PDX models; RCC-43b was derived from a metastatic PRCC and RCC-47 from a primary lesion and both patient samples displayed large cells with abundant eosinophilic cytoplasm, consistent with type II characteristics (13). Detailed GISTIC analysis of SNP 6.0 data demonstrated that both RCC-43b (passage number 6) and RCC-47 (passage number 5) had copy number gain of the region containing MET (Fig. 1A and B) with estimated copy numbers of 6 for each model. This relatively modest copy number gain is in line with recent CGH results showing MET copy number gain in 17 of 37 PRCC samples (46%) with none being MET amplified (defined as copy number gain by CGH above 5 copies; ref. 9). Additional chromosomal regions with copy number gain or loss were identified, including a region near the centromere of chromosome 7 amplified in the RCC-47 model (Fig. 1B). Using an independent platform for determining gene copy number (FISH), we determined that RCC-43b and RCC-47 carried 8 and 9 copies of MET, respectively. FISH analysis of the centromere probe CEP7 showed 3 copies in the RCC-43b model and 6 copies in the RCC-47 model, consistent with the finding of an amplicon on the p-arm side of the centromeric region in RCC-47 which allowed the CEP7 probe to hybridize. Consequently, the MET/CEP7 copy number ratio was 3.24 in RCC-43b and lower in RCC-47 (1.55) despite the fact that MET is amplified to a similar extent in both RCC-43b and RCC-47 models (Fig. 1C). Finally, presence of MET protein was readily detectable in both PRCC PDX models (Fig. 1D). A detailed survey of regions with copy number gain revealed that MET was the only known oncogene amplified in both models (Supplementary Table S1). To determine putative mutations, all exons of MET were sequenced using the BGI Illumina platform. No mutations in MET were detected in either model (Supplementary Table S2; 388× and 405× average coverage for RCC-43b and RCC-47, respectively). As the MET pathway can be activated by upregulation of HGF and HGFAC, we determined the expression of HGF and HGFAC. Expression of HGFAC transcript was detected in all models examined with no appreciable difference between the RCC models examined. Interestingly, expression of HGF was increased relative to other models in RCC-47 suggesting presence of a possible autocrine/paracrine stimulatory loop in this model (Supplementary Fig. S3). Together, these data show that RCC-43b and RCC-47 do not carry MET mutations, both contain regions of MET copy number gain, and that RCC47 shows overexpression of HGF mRNA consistent with genetic aberrations described in primary PRCC tumors, suggesting that these PDX models are representative of a subset of the PRCC patient population.

Characterization of sunitinib and crizotinib in RCC-43b and RCC-47

Given the poor response of PRCC patients to current therapies such as sunitinib (10) and the observations that high MET or HGF may confer resistance to antiangiogenic treatments like sunitinib (14), we speculated that the PDX models may not respond to the standard-of-care treatment. To begin benchmarking the antitumor activity of AZD6094, we treated RCC-43b tumor-bearing mice (passage number 9) with sunitinib at 10 and 80 mg/kg daily. The clinically active dose of sunitinib of 50 to 75 mg daily results in an AUC of approximately 1.5 μg·h/mL and a trough plasma concentration of approximately 68 ng/mL (15, 16). A dose of 10 mg/kg was chosen to achieve the clinically relevant AUC and a dose of 80 mg/kg was chosen to achieve the clinically relevant trough concentration based on published mouse pharmacokinetics (17, 18). Sunitinib dosed at the clinically relevant AUC of 10 mg/kg daily showed no signs of antitumor activity (∼10% tumor growth inhibition (TGI), $P > 0.05$ vs. vehicle), whereas antitumor activity was seen at 80 mg/kg daily (∼60% TGI, $P < 0.05$ vs. vehicle; Fig. 2A). Next, we sought to better understand whether crizotinib, an ALK/ROS/MET inhibitor currently FDA approved for ALK-positive NSCLC, would be more or less active than a MET-selective inhibitor in a model of PRCC. The clinically active dose of crizotinib of 250 mg results in an AUC of approximately 2.5–3.8 μg·h/mL (19). The pharmacokinetics of crizotinib in nude mice have been described showing a nonlinear relationship between dose and exposure across the dose range 2.5 to 50 mg/kg with 25 mg/kg resulting in an AUC exceeding that of human (4.7–5.7 μg·h/mL; ref. 20). We therefore treated RCC-47 tumor bearing mice (passage number 10) with a dose of 2.5 mg/kg daily and 25 mg/kg daily, the latter representing a preclinical dose exceeding the clinically achievable AUC exposures and expected to deliver >90% p-MET inhibition over the dosing interval (20, 21). Crizotinib dosed

Downloaded from clincancerres.aacrjournals.org on January 12, 2016. © 2015 American Association for Cancer Research.

Published OnlineFirst March 16, 2015; DOI: 10.1158/1078-0432.CCR-14-2685

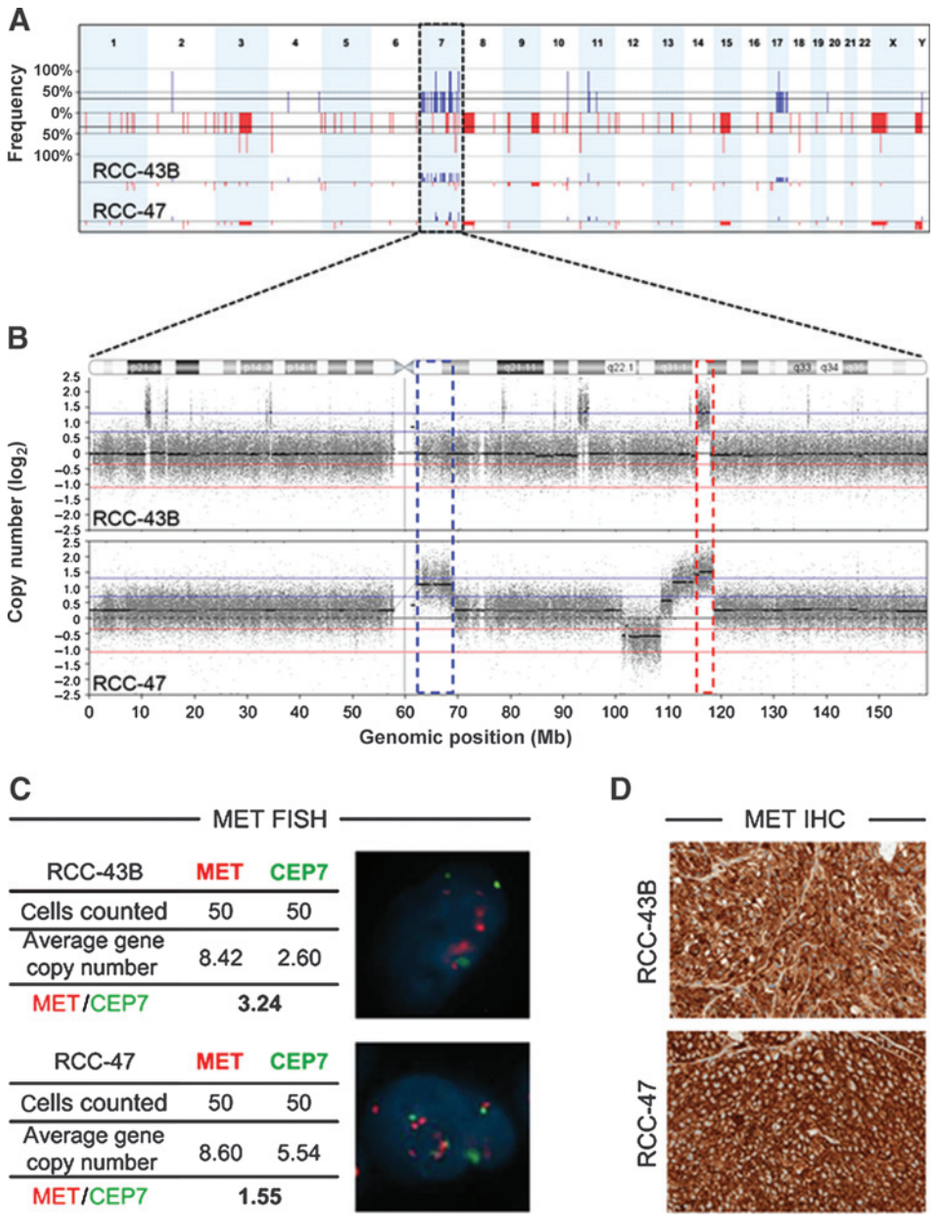

Figure 1.
MET amplification in RCC-43b and RCC-47. A, frequency plot summarizing amplifications and deletions across both models as defined in Materials and Methods. B, chromosome 7 log2 copy number plot. Each probe displayed as a small gray dot along the length of the chromosome. Two tier calling thresholds specified as gain (0.7), high copy gain(1.3) in blue, and loss (−0.35), high copy loss (−1.1) in red. Area highlighted represents region of high copy gain overlap containing the MET gene (Supplementary Table S1). Blue box denotes additional amplified region in RCC-47 containing CEP7. C, FISH with MET SpectrumRed/CEP7 Spectrum-Green probe set of patient derived PRCC (left) 60× images of a representative cell (right) where 50 cells were scored and an average probe copy number for both MET and CEP7 are tabulated. Both PRCC PDX models, RCC-43b (top) and RCC-47 (bottom) are shown to have MET gene copy number gain. D, immunohistochemistry (IHC) of MET in RCC-43b and RCC-47.

at 2.5 mg/kg daily showed no sign of antitumor activity (~11% TGI, $P > 0.05$ vs. vehicle). Crizotinib dosed at 25 mg/kg daily showed stasis for the first week of treatment, after which the tumors started to grow through treatment (Fig. 2B).

AZD6094 induces tumor regressions in RCC-43b and RCC-47

Based on the status of MET copy number in both PRCC PDX models and the HGF mRNA expression in RCC-47, we hypothesized that MET signaling could contribute significantly to the oncogene dependency of the tumor and that inhibition of MET signaling could lead to tumor growth inhibition. AZD6094 is a potent MET kinase inhibitor with >200-fold selectivity over 267 other kinases tested (12). Because no cell lines exist for the RCC-43b and RCC-47 PRCC models, we compared the potency of AZD6094 to sunitinib, crizotinib, and the MET inhibitors SGX-523, JNJ3887605, PHA-665752, and INC280 in the MET non-amplified and amplified gastric cancer cell lines AGS and GTL16 (Supplementary Fig. S1). Proliferation of the MET-amplified gastric cancer cell line GTL16 was inhibited by all MET inhibitors with INC280 and AZD6094 showing the highest potency (IC_{50} ~2 nmol/L and ~4 nmol/L, respectively). In contrast, none of the selective MET inhibitors showed activity in AGS consistent with the fact that AGS is not MET dependent. Crizotinib showed some activity in AGS, but with an IC_{50} significantly higher than seen in GTL16 (2.6 μmol/L vs. 28 nmol/L) presumably reflecting activity through another kinase (Supplementary Fig. S1). To test AZD6094 in this disease setting, we treated RCC-43b and RCC-47 tumor bearing mice with doses of AZD6094 up to 25 mg/kg daily. The upper dose chosen achieves an AUC exposure in mice equivalent to that achieved in man when dosed at 600 mg daily

Downloaded from clincancerres.aacrjournals.org on January 12, 2016. © 2015 American Association for Cancer Research.

Published OnlineFirst March 16, 2015; DOI: 10.1158/1078-0432.CCR-14-2685

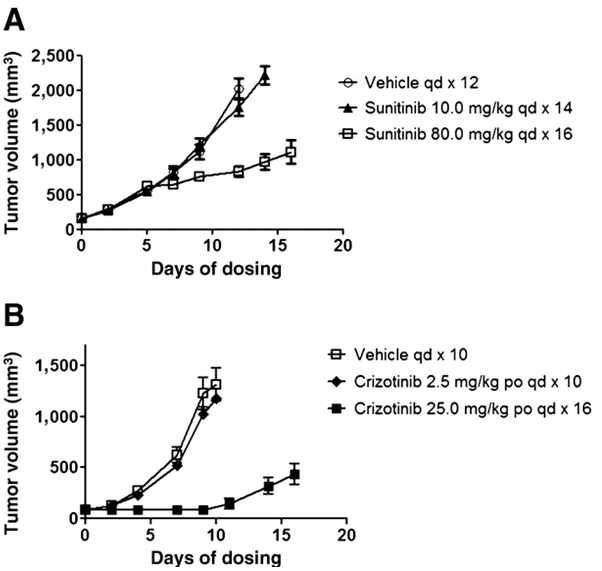

Figure 2.
Antitumor activity of sunitinib and crizotinib in RCC-43b and RCC-47, respectively. RCC-43b (A) or RCC-47 (B) tumor bearing mice were randomized in groups of $n = 10$ when average tumor volume reached ~100 mm^3. Daily oral administration of sunitinib, or crizotinib, at the indicated dose levels continued till the end of the study. Tumor volumes were measured on indicated days and graphed as mean tumor volume ± SEM.

(22). Doses tested are significantly lower than the maximum tolerated dose of AZD6094 in nude mice (~100 mg/kg daily). Consequently, AZD6094 did not induce body weight loss or other signs of adverse events (data not shown). AZD6094 dosed at 0.5, 2.5, 10, and 25 mg/kg daily induced dose dependent antitumor activity in RCC-47 resulting in approximately 63% TGI, ~89% TGI, ~64% regression, and ~96% regression, respectively (Fig. 3B). RCC-47 is a fast growing model, with animals in the vehicle group requiring sacrifice as early as 10 days after initiation of treatment. To determine whether AZD6094 induced a durable antitumor response, treatment was stopped after 16 days and tumors in the 25 mg/kg dose group were monitored for regrowth. Tumors grew back in 9 of 10 mice within 3 weeks after treatment was stopped; one mouse remained tumor free for 3 months (final measurement, results not shown). In RCC-43b, AZD6094 again showed a dose-dependent antitumor activity ranging from approximately 85% TGI when dosed at 2.5 mg/kg daily, stasis when dosed 10 mg/kg daily, and approximately 20% regression when dosed at 25 mg/kg daily. To determine whether activity to AZD6094 treatment changed after continued dosing, we extended the treatment to approximately 5 weeks. As shown in Fig. 3A, the antitumor activity of AZD6094 was maintained throughout the treatment period reaching approximately 28% regression in the 25 mg/kg daily group by the end of the study. In addition, there were no signs of accelerated growth throughout the treatment period, suggesting similar TGI is maintained throughout drug treatment with no obvious signs of resistance occurring. Comparing the antitumor activity of AZD6094 with that of sunitinib or that of crizotinib, each administered at its respective clinically achievable exposure, demonstrates that AZD6094 is more efficacious in these 2 PDX tumors of MET-amplified PRCC. To rule out potential changes in MET copy number between tumor passages used for genetic characterization and those used for pharmacodynamic and efficacy studies, we determined MET copy number in RCC-43 tumors from passage 6 and 9, and in RCC-47 tumors from passage 5 and 10 by qPCR. Both RCC-43b and RCC-47 had MET copy number of approximately 10 (Supplementary Fig. S2). Importantly, MET copy number was stable between tumor passages used.

Pharmacokinetic/pharmacodynamic/efficacy relationship of AZD6094 in RCC-43b and RCC-47

Constitutive activity of MET can influence both MAPK and AKT signaling and ultimately cell proliferation and survival, respectively. We postulated that MET inhibition would have dramatic effects on the downstream genes within these pathways and ultimately cell growth. To test this hypothesis, a pharmacokinetic/pharmacodynamic study was conducted in both RCC-43b and RCC-47 models to determine extent and duration of target and pathway modulation after a single dose of AZD6094. Tumor bearing mice ($n = 3$ per group per time point) received a single dose of AZD6094 of 0.5 (RCC-47 only), 2.5, 10, and 25 mg/kg and blood and tumors were collected 2, 8, and 24 hours after dosing. Pharmacokinetic analysis revealed dose proportional plasma exposure with a maximum concentration at 2 hours, and relatively fast clearance reaching nondetectable levels at 24 hours consistent with previously published rodent pharmacokinetic profiles (Fig. 4A).

In RCC-47, AZD6094 treatment resulted in near-complete inhibition of MET pY1349 2 hours after dosing (~95% inhibition relative to vehicle) even with the lowest dose administered. Eight hours after dosing, pY1349 levels were reduced by approximately 51% and 62% in the 0.5 and 2.5 mg/kg groups, respectively and by

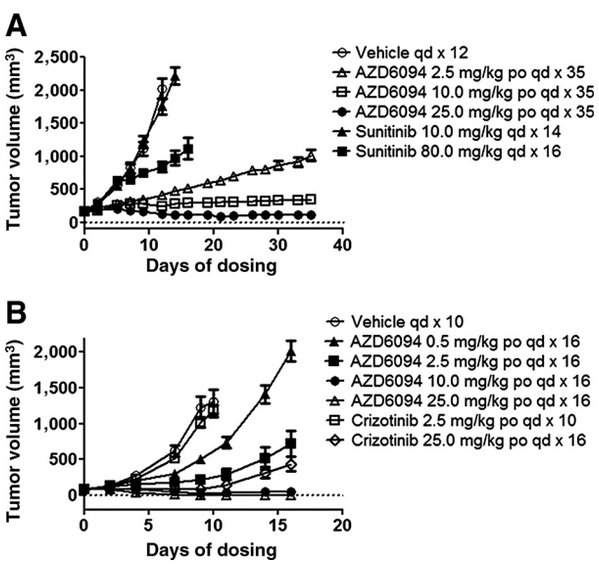

Figure 3.
AZD6094 displays single-agent dose-dependent antitumor activity in RCC-43b and RCC-47 and is more efficacious than sunitinib or crizotinib in RCC-47 (B) or RCC-43b (A) tumor bearing mice were randomized in groups of $n = 10$ when average tumor volume reached ~100 mm^3. Daily oral administration of AZD6094, sunitinib, or crizotinib at the indicated dose levels continued till the end of the study. Tumor volumes were measured on indicated days and graphed as mean tumor volume ± SEM.

Downloaded from clincancerres.aacrjournals.org on January 12, 2016. © 2015 American Association for Cancer Research.

Published OnlineFirst March 16, 2015; DOI: 10.1158/1078-0432.CCR-14-2685

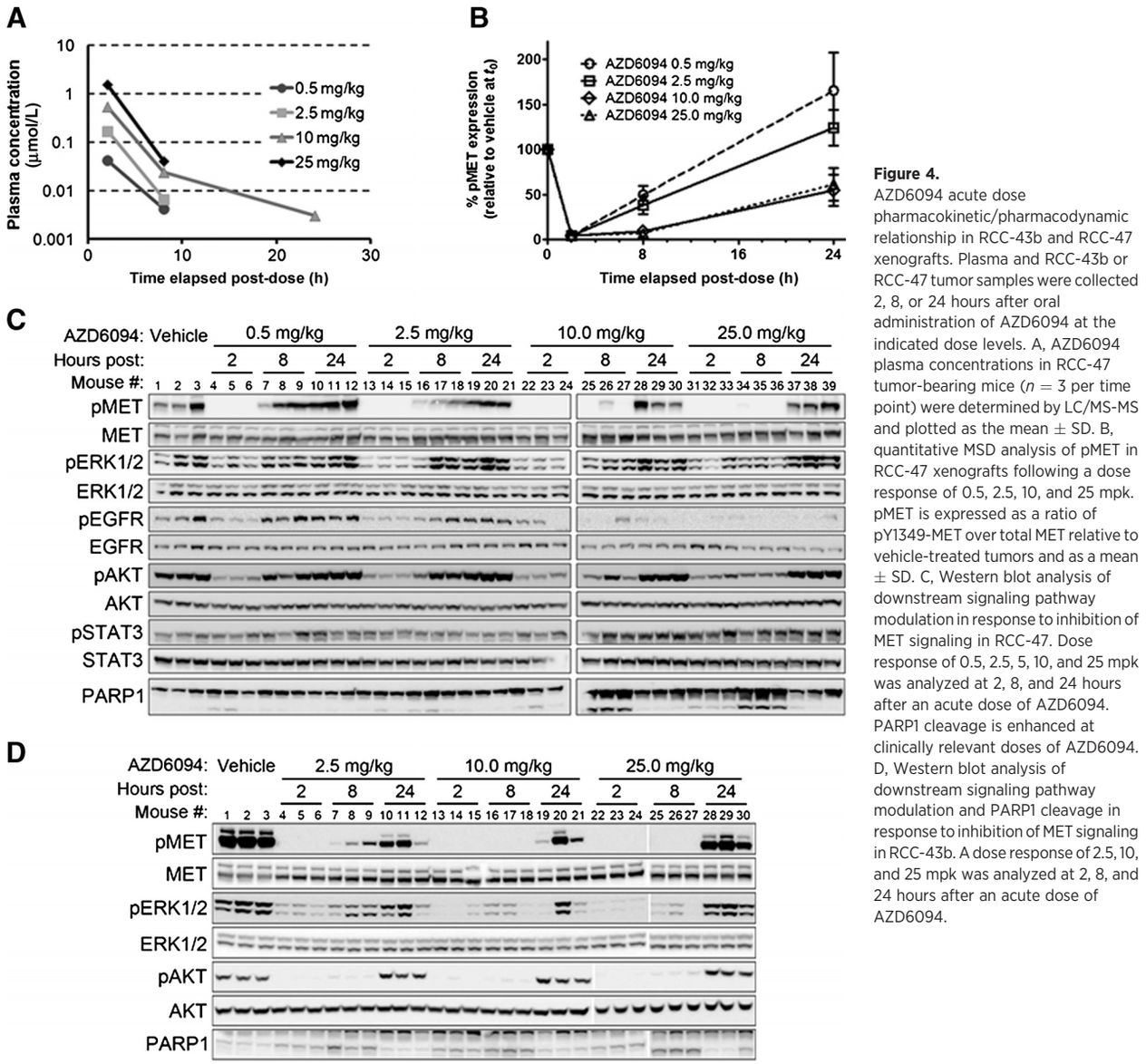

Figure 4.
AZD6094 acute dose pharmacokinetic/pharmacodynamic relationship in RCC-43b and RCC-47 xenografts. Plasma and RCC-43b or RCC-47 tumor samples were collected 2, 8, or 24 hours after oral administration of AZD6094 at the indicated dose levels. A, AZD6094 plasma concentrations in RCC-47 tumor-bearing mice ($n = 3$ per time point) were determined by LC/MS-MS and plotted as the mean ± SD. B, quantitative MSD analysis of pMET in RCC-47 xenografts following a dose response of 0.5, 2.5, 10, and 25 mpk. pMET is expressed as a ratio of pY1349-MET over total MET relative to vehicle-treated tumors and as a mean ± SD. C, Western blot analysis of downstream signaling pathway modulation in response to inhibition of MET signaling in RCC-47. Dose response of 0.5, 2.5, 5, 10, and 25 mpk was analyzed at 2, 8, and 24 hours after an acute dose of AZD6094. PARP1 cleavage is enhanced at clinically relevant doses of AZD6094. D, Western blot analysis of downstream signaling pathway modulation and PARP1 cleavage in response to inhibition of MET signaling in RCC-43b. A dose response of 2.5, 10, and 25 mpk was analyzed at 2, 8, and 24 hours after an acute dose of AZD6094.

approximately 90% and 93% in the 10 and 25 mg/kg groups, respectively. By 24 hours, p-Y1349 was back to baseline in the 0.5 and 2.5 mg/kg groups (~166% and ~124%, $P > 0.05$ vs. vehicle), whereas pY1349 was still inhibited by approximately 45% and 39% in the 10 and 25 mg/kg groups, respectively (Fig. 4B). Western blot analysis revealed a similar profile of p-Y1234/5 MET inhibition with complete inhibition seen at 2 hours across all doses, and a dose-dependent duration of inhibition with near-complete inhibition retained up to 8 hours only in the 10 and 25 mg/kg dose groups (Fig. 4C). Analysis of downstream signaling pathways revealed that AZD6094 resulted in significant, but not complete, inhibition of p-ERK (Thr202/Tyr204) and p-AKT (S473). No significant changes were observed in p-STAT3 signal (Y705) in contrast to recent observations in gastric cancer (23). AZD6094 induced dose- and time-dependent downregulation of p-EGFR consistent with earlier reports describing cross-talk between MET and EGFR (24, 25). AZD6094 treatment resulted in a dose- and time-dependent increase in cleaved PARP1, indicative of activation of apoptotic signaling, and was most prominent after 8 hours in the 10 mg/kg or 25 mg/kg dose groups (Fig. 4C).

In RCC-43b, AZD6094 showed a similar pattern of pMET inhibition with complete pMET inhibition at 2 hours across all dose groups tested, and a dose-related duration of pMET inhibition (Fig. 4D).

In summary, duration of pMET inhibition correlated with antitumor activity in RCC-47 and inhibition of downstream signaling. Interestingly, MET inhibition resulting in antitumor activity correlated with PARP cleavage in tumor samples, suggesting a robust functional cell death response.

Crizotinib shows less pathway inhibition in RCC-47

To gain a deeper understanding of differences in antitumor activity between crizotinib and AZD6094, we determined pMET levels at the end of the efficacy study (after 16 days treatment).

Downloaded from clincancerres.aacrjournals.org on January 12, 2016. © 2015 American Association for Cancer Research.

Published OnlineFirst March 16, 2015; DOI: 10.1158/1078-0432.CCR-14-2685

Tumor samples collected 2 hours after the final dose of crizotinib showed a dose-dependent inhibition of pMET. However, pMET signal was still detectable in the 25 mg/kg crizotinib group (89.3% ± 3.7% inhibition) indicating crizotinib at this dose did not block MET signaling completely. In contrast, tumor samples taken from the AZD6094 2.5 mg/kg group did show complete inhibition of pMET signal (99.8% ± 0.3%, Fig. 5). AZD6094 at 10 mg/kg daily and 25 mg/kg daily resulted in near-complete tumor regressions leaving insufficient material for pharmacodynamic analysis.

Twice a day dosing increased antitumor activity in RCC-47

The notion that pMET was no longer completely inhibited 8 hours after dosing the 0.5 mg/kg and 2.5 mg/kg groups raised the question whether a second dose, presumably prolonging exposure of AZD6094, would increase antitumor activity. RCC-47 bearing mice were therefore treated with 1.25 mg/kg twice a day and 12.5 mg/kg twice a day (same total amount of drug as 2.5 mg/kg daily and 25 mg/kg daily, respectively). The second dose was administered 8 hours after the first dose, a time where plasma exposure to AZD6094 was approximately 7 nmol/L in the 2.5 mg/kg group and approximately 43 nmol/L in the 25 mg/kg group. The 1.25 mg/kg twice a day dose resulted in significantly greater antitumor activity than the 2.5 mg/kg daily group, reaching approximately 8% regression compared with 89% TGI after 9 days of treatment (Fig. 6). As shown previously, the 25 mg/kg daily group resulted in near complete regressions, and 12.5 mg/kg twice a day treatment showed equivalent antitumor activities (~88% regression vs. ~96% regression, $P > 0.05$).

Discussion

Advanced PRCC remains a disease with a high unmet medical need with the current standard-of-care delivering only limited clinical benefit (10). The evaluation and development of novel therapeutics is further hampered by the lack of suitable *in vitro* and *in vivo* model systems. Here we describe the use of two PRCC PDX models, RCC-43b and RCC-47 (13, 26). Detailed aCGH and FISH analysis confirmed that both PRCC PDX models are wild-type for MET and have increased MET copy number. In addition, one displays increased HGF expression levels suggesting presence of a putative autocrine/paracrine activation loop. Together, these data suggest that these models may be representative of a subset of PRCC patients and may therefore represent models that can better predict clinical efficacy (9).

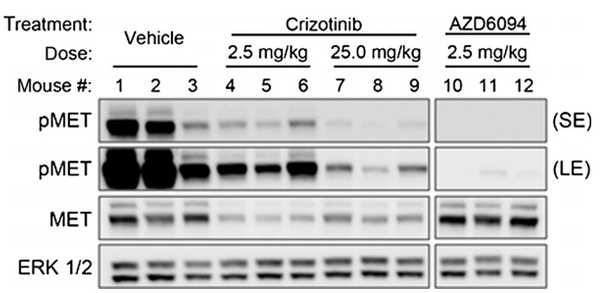

Figure 5.
Crizotinib and AZD6094 end of study pharmacodynamics in RCC-47 xenografts. Western blot analysis of downstream signaling pathway modulation in response to inhibition of MET signaling. RCC-47 tumor samples were collected 2 hours after final oral administration of crizotinib or AZD6094 at the indicated dose levels.

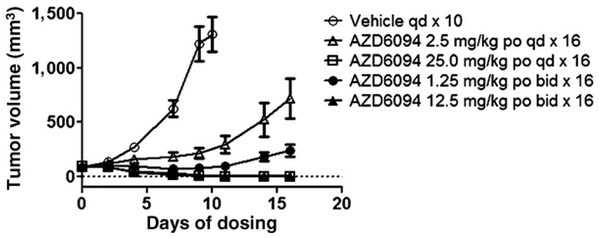

Figure 6.
Twice a day dosing of AZD6094 is more efficacious than daily dosing in RCC-47. RCC-47 tumor bearing mice were randomized in groups of $n = 10$ when average tumor volume reached ~100 mm^3. AZD6094 was administered daily or twice a day (8 hours;16-hour schedule) at the indicated dose levels till the end of the study. Tumor volumes were measured on indicated days and graphed as mean tumor volume ± SEM.

AZD6094 is a novel, selective, and potent small-molecule MET inhibitor (12). Evaluating the activity of AZD6094 in two independent PRCC PDX models revealed robust dose-dependent single-agent antitumor activity resulting in tumor regressions in both PRCC PDX models when dosed at the clinically relevant dose of 25 mg/kg daily (matched to the AUC exposure in man dosed 600 mg daily; 22). Interestingly, continued dosing of AZD6094 for approximately 5 weeks showed continuous antitumor activities with no signs of emergent resistance. These findings are significant as they present for the first time preclinical data of a MET inhibitor in preclinical models of PRCC. In contrast, the RCC standard-of-care sunitinib showed no signs of antitumor activity when dosed at clinically matched AUC exposures (15). Sunitinib doses targeting to maintain the trough concentration reported in man (15) did show significant antitumor activity although not resulting in regressions as seen with AZD6094. These findings are in line with previous reports indicating MET signaling as a sunitinib resistance mechanism (14) and suggest that AZD6094 could be of therapeutic potential in sunitinib-resistant PRCC patients.

Multikinase inhibitors targeting MET could be of potential utility in MET-driven disease and crizotinib has been reported to be effective in sunitinib-resistant tumors with MET involvement (27). We therefore compared the activity of the FDA-approved ALK/ROS/MET multikinase inhibitor crizotinib to the selective MET inhibitor AZD6094. At clinically relevant AUC exposures (expected to deliver >90% pMET inhibition over the dosing interval; ref. 20), crizotinib indeed displayed an antitumor response maintaining tumor stasis during the first 9 days of treatment. However, tumors grew through treatment after 9 days. This is in stark contrast to the near complete tumor regressions obtained with AZD6094. Comparing samples obtained at the end of the efficacy study revealed that crizotinib treatment inhibited pMET to a lesser degree than AZD6094. Thus, it would seem that the potency of crizotinib to inhibit MET signaling, or its clinically relevant dose, limits its antitumor activity in the PRCC PDX model. Interestingly, AZD6094 did show increased potency over crizotinib in the MET-amplified gastric cell line GTL16, whereas other selective MET inhibitors were equipotent. This suggests that potent and selective MET inhibitors may be more effective in treating MET-driven disease.

The pharmacodynamic response to AZD6094 revealed that at the earliest time point measured, pMET was inhibited to the same extent at all dose levels tested, including dose levels that showed suboptimal antitumor activity. A dose relationship in pMET

Downloaded from clincancerres.aacrjournals.org on January 12, 2016. © 2015 American Association for Cancer Research.

Published OnlineFirst March 16, 2015; DOI: 10.1158/1078-0432.CCR-14-2685

inhibition was only seen at the later time points. Dose levels that resulted in suboptimal antitumor activity in RCC-47, showed pMET levels returning by 8 hours, whereas dose levels inducing tumor regression maintained their pMET inhibition for at least 8 hours. Interestingly, by 8 hours, AZD6094 treatment in RCC-47 also resulted in PARP cleavage, indicative of activation of apoptotic signaling, but only in the dose groups that resulted in tumor regressions. The correlation between induction of PARP cleavage and regression was less clear in RCC-43b possibly due to differences in growth and response kinetics between the two models. However, the dose relationship between duration of pMET inhibition and antitumor activity remained. Taken together, these data suggest that increasing the duration of pMET inhibition increases the antitumor activity in PRCC PDX models. Indeed, treating tumor bearing mice twice a day with the same total amount of drug resulted in increased antitumor activity.

While the availability of these PRCC PDX models enabled us to test our selective MET inhibitor in a MET-amplified setting, the identification of models representing MET mutations are still of great interest. Clinical reports from the dual MET/VEGFR2 inhibitor foretinib phase II trial and a case report from a patient treated with the investigational selective MET inhibitor PF-0417903 suggest that MET inhibition will be efficacious in patients harboring germline MET mutations (28, 29); however, further evaluation of newly described mutations (9) as well as testing of the activity of other selective MET inhibitors against these mutations will be necessary.

The finding that AZD6094 induces single-agent regressions in these PRCC models raises the question whether AZD6094 could have potential activity in other disease settings. MET is amplified in gastric cancer and NSCLC and single-agent antitumor activity of AZD6094 (savolitinib, HMPL-504) has been described in preclinical xenograft models (30, 31). Moreover, MET amplification has been described in settings of resistance. For example, in NSCLC, gefitinib-resistant HCC827 cells gained MET amplification and responded to the combination of gefitinib and the MET inhibitor PHA-665752. Interestingly, MET amplification was also detected in up to 22% of clinical specimen of gefitinib- or erlotinib-resistant lung cancer patients (32). In colorectal cancer, MET amplification has been linked to *de novo* and acquired resistance of cetuximab with cetuximab-resistant tumor models retaining single agent or combination activity to crizotinib or the MET inhibitor JNJ-38877605 (33, 34). Also, MET and HGF overexpression can occur in the absence of gene amplification as described in renal, thyroid, and ovarian cancers (4, 35, 36). Thus, selective MET inhibitors such as AZD6094 could have clinical utility in indications outside of PRCC and may provide therapeutic means to delay or overcome resistance to EGFR-targeted strategies.

Recently, clinical proof-of-concept for targeting MET in PRCC has emerged. A patient with metastatic PRCC showed a partial response to the selective MET inhibitor PF-04217903 lasting 26 months. Interestingly, sequencing of archival tissue revealed an activating M1268T mutation in MET (29). In addition, phase II clinical studies of the dual MET/VEGFR2 inhibitor foretinib demonstrated an overall response rate by RECIST criteria of 13.5%. Importantly, five of 10 responders carried a germline MET mutations and was highly predictive of response (28). Finally, in an early clinical dose escalation study, AZD6094 demonstrated partial responses in 3 PRCC patients, with a fourth patient still on study reaching 27% tumor reduction. Analysis of pretreatment PRCC tumor samples showed that the responders had either MET gene copy number increase or high MET protein expression (22). Taken together, these data warrant further development of MET inhibitors in PRCC.

Disclosure of Potential Conflicts of Interest

M. Zinda has ownership interest (including patents) in AstraZeneca. No potential conflicts of interest were disclosed by the other authors.

Authors' Contributions

Conception and design: A.G. Schuller, M.M. Frigault, A. Adam, M. Zinda, E.A. Clark, C.M. D'Cruz

Development of methodology: A. Smith

Acquisition of data (provided animals, acquired and managed patients, provided facilities, etc.): R.E. Henry, M. Hattersley, A. Smith, O. Déas, D. Nicolle, A. Adam

Analysis and interpretation of data (e.g., statistical analysis, biostatistics, computational analysis): A.G. Schuller, E. Barry, R.D.O. Jones, G. Beran, D. Linsenmayer, A. Smith, J. Wilson, S. Cairo, A. Adam, M. Zinda, C. Reimer, E.A. Clark, C.M. D'Cruz

Writing, review, and/or revision of the manuscript: A.G. Schuller, E.R. Barry, R.D.O. Jones, M.M. Frigault, G. Beran, A. Smith, S. Cairo, D. Nicolle, M. Zinda, C. Reimer, E.A. Clark, C.M. D'Cruz

Administrative, technical, or material support (i.e., reporting or organizing data, constructing databases): M.M. Frigault, S. Cairo, O. Déas, D. Nicolle

Study supervision: A.G. Schuller, D. Nicolle, C. Reimer, S.E. Fawell, C.M. D'Cruz

Acknowledgments

The authors thank Dr. Steven Brunelli for critical reading of the article.

The costs of publication of this article were defrayed in part by the payment of page charges. This article must therefore be hereby marked *advertisement* in accordance with 18 U.S.C. Section 1734 solely to indicate this fact.

Received October 16, 2014; revised February 12, 2015; accepted March 5, 2015; published OnlineFirst March 16, 2015.

References

1. Birchmeier C, Birchmeier W, Gherardi E, Vande Woude GF. Met, metastasis, motility and more. Nat Rev Mol Cell Biol 2003;4:915–25.
2. Corso S, Comoglio PM, Giordano S. Cancer therapy: can the challenge be MET? Trends Mol Med 2005;11:284–92.
3. Gherardi E, Birchmeier W, Birchmeier C, Vande Woude G. Targeting MET in cancer: rationale and progress. Nat Rev Cancer 2012;12:89–103.
4. Giubellino A, Linehan WM, Bottaro DP. Targeting the Met signaling pathway in renal cancer. Expert Rev Anticancer Ther 2009;9:785–93.
5. Tanizaki J, Okamoto I, Sakai K, Nakagawa K. Differential roles of transphosphorylated EGFR, HER2, HER3, and RET as heterodimerisation partners of MET in lung cancer with MET amplification. Br J Cancer 2011; 105:807–13.
6. Chow WH, Devesa SS. Contemporary epidemiology of renal cell cancer. Cancer J 2008;14:288–301.
7. Kovacs G. Molecular cytogenetics of renal cell tumors. Adv Cancer Res 1993;62:89–124.
8. Lubensky IA, Schmidt L, Zhuang Z, Weirich G, Pack S, Zambrano N, et al. Hereditary and sporadic papillary renal carcinomas with c-met mutations share a distinct morphological phenotype. Am J Pathol 1999; 155:517–26.
9. Albiges L, Guegan J, Le Formal A, Verkarre V, Rioux-Leclercq N, Sibony M, et al. MET is a potential target across all papillary renal cell carcinomas: result from a large molecular study of pRCC with CGH array and matching gene expression array. Clin Cancer Res 2014;20:3411–21.

Downloaded from clincancerres.aacrjournals.org on January 12, 2016. © 2015 American Association for Cancer Research.

Published OnlineFirst March 16, 2015; DOI: 10.1158/1078-0432.CCR-14-2685

10. Gore ME, Szczylik C, Porta C, Bracarda S, Bjarnason GA, Oudard S, et al. Safety and efficacy of sunitinib for metastatic renal-cell carcinoma: an expanded-access trial. Lancet Oncol 2009;10:757–63.
11. Jia H, Dai G, Weng J, Zhang Z, Wang Q, Zhou F, et al. Discovery of (S)-1-(1-(Imidazo[1,2-a]pyridin-6-yl)ethyl)-6-(1-methyl-1H-pyrazol-4-yl)-1H-[1,2, 3]triazolo[4,5-b]pyrazine (volitinib) as a highly potent and selective mesenchymal-epithelial transition factor (c-Met) inhibitor in clinical development for treatment of cancer. J Med Chem 2014;57:7577–89.
12. Gavine PR, Ren Y, Han L, Lv J, Fan S, Zhang W, et al. Volitinib, a potent and highly selective c-Met inhibitor, effectively blocks c-Met signaling and growth in c-MET amplified gastric cancer patient-derived tumor xenograft models. Mol Oncol 2015;9:323–33.
13. Glukhova L, Goguel AF, Chudoba I, Angevin E, Pavon C, Terrier-Lacombe MJ, et al. Overrepresentation of 7q31 and 17q in renal cell carcinomas. Genes Chromosomes Cancer 1998;22:171–8.
14. Shojaei F, Lee JH, Simmons BH, Wong A, Esparza CO, Plumlee PA, et al. HGF/c-Met acts as an alternative angiogenic pathway in sunitinib-resistant tumors. Cancer Res 2010;70:10090–100.
15. Houk BE, Bello CL, Poland B, Rosen LS, Demetri GD, Motzer RJ. Relationship between exposure to sunitinib and efficacy and tolerability endpoints in patients with cancer: results of a pharmacokinetic/pharmacodynamic meta-analysis. Cancer Chemother Pharmacol 2010;66:357–71.
16. Mendel DB, Laird AD, Xin X, Louie SG, Christensen JG, Li G, et al. In vivo antitumor activity of SU11248, a novel tyrosine kinase inhibitor targeting vascular endothelial growth factor and platelet-derived growth factor receptors: determination of a pharmacokinetic/pharmacodynamic relationship. Clin Cancer Res 2003;9:327–37.
17. Zhou Q, Gallo JM. Quantification of sunitinib in mouse plasma, brain tumor and normal brain using liquid chromatography-electrospray ionization-tandem mass spectrometry and pharmacokinetic application. J Pharm Biomed Anal 2010;51:958–64.
18. Haznedar JO, Patyna S, Bello CL, Peng GW, Speed W, Yu X, et al. Single- and multiple-dose disposition kinetics of sunitinib malate, a multitargeted receptor tyrosine kinase inhibitor: comparative plasma kinetics in nonclinical species. Cancer Chemother Pharmacol 2009;64:691–706.
19. Timm A, Kolesar JM. Crizotinib for the treatment of non-small-cell lung cancer. Am J Health Syst Pharm 2013;70:943–7.
20. Yamazaki S, Skaptason J, Romero D, Lee JH, Zou HY, Christensen JG, et al. Pharmacokinetic-pharmacodynamic modeling of biomarker response and tumor growth inhibition to an orally available cMet kinase inhibitor in human tumor xenograft mouse models. Drug Metab Dispos 2008; 36:1267–74.
21. Yamazaki S, Skaptason J, Romero D, Vekich S, Jones HM, Tan W, et al. Prediction of oral pharmacokinetics of cMet kinase inhibitors in humans: physiologically based pharmacokinetic model versus traditional one-compartment model. Drug Metab Dispos 2011;39:383–93.
22. Hui Kong Gan JL, Michael Millward, Yi Gu, Weiguo SU, Melanie Frigault, Chuan Qi, et al. First-in-human phase I study of a selective c-Met inhibitor volitinib (HMP504/AZD6094) in patients with advanced solid tumors. J Clin Oncol 2014;32:(suppl; abstr 11111).
23. Lai AZ, Cory S, Zhao H, Gigoux M, Monast A, Guiot MC, et al. Dynamic reprogramming of signaling upon met inhibition reveals a mechanism of drug resistance in gastric cancer. Sci Signal 2014;7:ra38.
24. Shattuck DL, Miller JK, Carraway KL III, Sweeney C. Met receptor contributes to trastuzumab resistance of Her2-overexpressing breast cancer cells. Cancer Res 2008;68:1471–7.
25. Dulak AM, Gubish CT, Stabile LP, Henry C, Siegfried JM. HGF-independent potentiation of EGFR action by c-Met. Oncogene 2011;30: 3625–35.
26. Glukhova L, Lavialle C, Fauvet D, Chudoba I, Danglot G, Angevin E, et al. Mapping of the 7q31 subregion common to the small chromosome 7 derivatives from two sporadic papillary renal cell carcinomas: increased copy number and overexpression of the MET proto-oncogene. Oncogene 2000;19:754–61.
27. Shojaei F, Simmons BH, Lee JH, Lappin PB, Christensen JG. HGF/c-Met pathway is one of the mediators of sunitinib-induced tumor cell type-dependent metastasis. Cancer Lett 2012;320:48–55.
28. Choueiri TK, Vaishampayan U, Rosenberg JE, Logan TF, Harzstark AL, Bukowski RM, et al. Phase II and biomarker study of the dual MET/VEGFR2 inhibitor foretinib in patients with papillary renal cell carcinoma. J Clin Oncol 2013;31:181–6.
29. Diamond JR, Salgia R, Varella-Garcia M, Kanteti R, LoRusso PM, Clark JW, et al. Initial clinical sensitivity and acquired resistance to MET inhibition in MET-mutated papillary renal cell carcinoma. J Clin Oncol 2013;31: e254–8.
30. Gavine PR, Ren Y, Han L, Lv J, Fan S, Zhang W, et al. Volitinib, a potent and highly selective c-Met inhibitor, effectively blocks c-Met signaling and growth in gastric cancer patient-derived tumor xenograft models. Mol Oncol 2015;9:323–33.
31. Yumin Cui GD, Ren Yongxin, Zhou Feng, Fan Shiming, Sai Yang, Gu Yi, et al. A novel and selective c-Met inhibitor against subcutaneous xenograft and othotopic brain tumor models. Cancer Res 2011;71.
32. Engelman JA, Zejnullahu K, Mitsudomi T, Song Y, Hyland C, Park JO, et al. MET amplification leads to gefitinib resistance in lung cancer by activating ERBB3 signaling. Science 2007;316:1039–43.
33. Van Emburgh BO, Sartore-Bianchi A, Di Nicolantonio F, Siena S, Bardelli A. Acquired resistance to EGFR-targeted therapies in colorectal cancer. Mol Oncol 2014;8:1084–94.
34. Bardelli A, Corso S, Bertotti A, Hobor S, Valtorta E, Siravegna G, et al. Amplification of the MET receptor drives resistance to anti-EGFR therapies in colorectal cancer. Cancer Discov 2013;3:658–73.
35. Mariani M, McHugh M, Petrillo M, Sieber S, He S, Andreoli M, et al. HGF/c-Met axis drives cancer aggressiveness in the neo-adjuvant setting of ovarian cancer. Oncotarget 2014;5:4855–67.
36. Ruco L, Scarpino S. The pathogenetic role of the HGF/c-Met system in papillary carcinoma of the thyroid. Biomedicines 2014;2:263–74.

Downloaded from clincancerres.aacrjournals.org on January 12, 2016. © 2015 American Association for Cancer Research.

Published OnlineFirst March 16, 2015; DOI: 10.1158/1078-0432.CCR-14-2685

AACR American Association for Cancer Research

Clinical Cancer Research

The MET Inhibitor AZD6094 (Savolitinib, HMPL-504) Induces Regression in Papillary Renal Cell Carcinoma Patient–Derived Xenograft Models

Alwin G. Schuller, Evan R. Barry, Rhys D.O. Jones, et al.

Clin Cancer Res 2015;21:2811-2819. Published OnlineFirst March 16, 2015.

Updated version	Access the most recent version of this article at: doi:10.1158/1078-0432.CCR-14-2685
Supplementary Material	Access the most recent supplemental material at: http://clincancerres.aacrjournals.org/content/suppl/2015/03/18/1078-0432.CCR-14-2685.DC1.html

Cited articles	This article cites 34 articles, 12 of which you can access for free at: http://clincancerres.aacrjournals.org/content/21/12/2811.full.html#ref-list-1

E-mail alerts	Sign up to receive free email-alerts related to this article or journal.
Reprints and Subscriptions	To order reprints of this article or to subscribe to the journal, contact the AACR Publications Department at pubs@aacr.org.
Permissions	To request permission to re-use all or part of this article, contact the AACR Publications Department at permissions@aacr.org.

Downloaded from clincancerres.aacrjournals.org on January 12, 2016. © 2015 American Association for Cancer Research.